Atmos. Chem. Phys. Discuss., https://doi.org/10.5194/acp-2018-202
Manuscript under review for journal Atmos. Chem. Phys.
Discussion started: 28 February 2018

Atmospheric Chemistry and Physics Discussions

On the discrepancy of HCl processing in the dark polar vortices

Jens-Uwe Grooß[1], Rolf Müller[1], Reinhold Spang[1], Ines Tritscher[1], Tobias Wegner[1,2], Martyn P. Chipperfield[3], Wuhu Feng[3,4], Douglas E. Kinnison[5], and Sasha Madronich[5]

[1]Institut für Energie- und Klimaforschung – Stratosphäre (IEK-7), Forschungszentrum Jülich, Germany
[2]now at: ifb AG Essen, Germany
[3]School of Earth and Environment, University of Leeds, UK
[4]National Centre for Atmospheric Science, University of Leeds, Leeds, UK
[5]Atmospheric Chemistry Observations and Modeling Laboratory, National Center for Atmospheric Research, Boulder, USA

Correspondence: Jens-Uwe Grooß (j.-u.grooss@fz-juelich.de)

Abstract.

More than three decades after the discovery of the ozone hole, the processes involved in its formation are believed to be understood in great detail. Current state-of-the-art models are able to reproduce the observed chemical composition in the springtime polar stratosphere, especially regarding the quantification of halogen-catalysed ozone loss. However, here we report on a discrepancy between simulations and observations during the less-well studied period of the onset of chlorine activation. During this period, which in the Antarctic is between May and July, model simulations significantly overestimate HCl, one of the key chemical species, inside the polar vortex during polar night. This HCl discrepancy is also observed in the Arctic and present, to varying extents, in three independent models, the Lagrangian chemistry transport model CLaMS as well as the Eulerian models WACCM and TOMCAT/SLIMCAT. The HCl discrepancy points to some unknown process in the formulation of stratospheric chemistry that is currently not represented in the models.

Here we characterise the HCl discrepancy in space and time for the Lagrangian Chemistry Transport Model CLaMS, in which HCl in the polar vortex core stays about constant from June to August in the Antarctic while the observations indicate a continuous HCl decrease over this period. The somewhat smaller discrepancies in the models WACCM and TOMCAT/SLIMCAT are also presented. Numerical diffusion in the Eulerian models is identified to be a likely cause for the inter-model differences. Although the missing process has not yet been identified, we investigate different hypotheses on the basis of the characteristics of the discrepancy. An under-estimated uptake of HCl into the PSC particles that consist mainly of H_2O and HNO_3 cannot explain the discrepancy due to the temperature correlation of the discrepancy. Also, a direct photolysis of particulate HNO_3 does not explain the discrepancy since it would also cause changes in late winter which are not observed. The ionisation caused by Galactic Cosmic Rays provides an additional NO_x and HO_x source that can explain only around 20% of the discrepancy. A hypothetical decomposition of particulate HNO_3 by some other process not dependent on the solar elevation, e.g. involving Galactic Cosmic Rays, may be a possible mechanism to resolve the HCl discrepancy. Since the discrepancy reported here occurs during the beginning of the chlorine activation period, where the ozone loss rates are slow, there is only a minor impact of about 2% on the overall ozone column loss over the course of Antarctic winter and spring.

Atmos. Chem. Phys. Discuss., https://doi.org/10.5194/acp-2018-202
Manuscript under review for journal Atmos. Chem. Phys.
Discussion started: 28 February 2018

Atmospheric Chemistry and Physics Discussions

1 Introduction

The discovery of large ozone depletion in the Antarctic spring, now known as the ozone hole (Farman et al., 1985; Stolarski et al., 1986) came as a complete surprise, although the effect of chlorine-catalysed ozone depletion had been discussed before (Molina and Rowland, 1974). Nevertheless the processes leading to the formation of the ozone hole were identified rather quickly after the discovery (Solomon et al., 1986) and now the involved processes are clarified in great detail (e.g. Solomon, 1999). Briefly, (1) the decomposition of anthropogenically emitted chlorofluorocarbons (CFCs) releases chlorine in the stratosphere, that are at first converted into the passive non-ozone-depleting compounds HCl and $ClONO_2$. (2) Polar stratospheric clouds (PSCs) form at the very low temperatures in the polar winter and spring. These are liquid or crystalline particles that mainly of condensed HNO_3 and H_2O that are taken up from the gas phase. The PSC particles, as well as the cold stratospheric sulphate aerosol, provide surfaces on which heterogeneous chemical reactions can occur. (3) The passive chlorine reservoir species HCl and $ClONO_2$ are activated into Cl_2 and HOCl by heterogeneous reactions on the PSCs and on the cold aerosols. The heterogeneous reaction of HCl with $ClONO_2$ plays the major role in this chlorine activation process. (4) In the presence of sunlight in polar spring, ozone is depleted by catalytic cycles involving the active chlorine compounds. There are also catalytic ozone depletion cycles involving bromine compounds. (5) Ozone-depleted air-masses are trapped within the polar vortex due to the efficient dynamical transport barrier at the polar vortex edge (Schoeberl and Hartmann, 1991).

Since the first explanation of the ozone hole, many research activities have focused on the detailed processes and on a quantitative numerical simulations of the ozone depletion mechanisms. Research activities include observations and simulations of gas-phase kinetics, heterogeneous chemistry, catalytic ozone loss cycles, liquid and solid PSC formation, PSC sedimentation and transport barriers at the polar vortex edge. Today it is known that there is a variety of particles present at low temperatures in the polar vortices (e.g. Pitts et al., 2011; Spang et al., 2017), ice particles of different sizes and number densities, nitric acid trihydrate particles (NAT), liquid super-cooled ternary $H_2SO_4/H_2O/HNO_3$ solution particles (STS) and cold binary sulphate aerosol. All of these particles can, in principle, facilitate the heterogeneous reactions that lead to an activation of chlorine in the polar stratosphere (Peter, 1997; Solomon, 1999; Wegner et al., 2012; Drdla and Müller, 2012; Shi et al., 2001; Grooß et al., 2011). An important impact of the PSCs is the uptake of HNO_3 into the particles which deplete the gas-phase of NO_x as long as the particles exist (Crutzen and Arnold, 1986; Müller et al., 2017). Particles like NAT, present in low number densities and in turn large sizes, are also able to transport downward significant amounts of reactive nitrogen NO_y resulting in denitrification of the stratospheric air (Fahey et al., 2001; Grooß et al., 2005).

These processes are introduced in state-of-the-art models that are able to reproduce the polar ozone depletion. Therefore, WMO (2014) states that “well understood stratospheric chemical processes involving chlorine and bromine are the primary cause of the seasonal polar ozone depletion". However, during the phase of initial chlorine activation in the polar vortices that has not yet been studied in sufficient detail, there is a difference in HCl between the simulations and observations that has not yet been reported. Here we report on a discrepancy between observations and simulations of HCl in the polar stratosphere during the period of initial chlorine activation in the core of the polar vortex that was first recognised by Wegner (2013). In the polar vortex stratosphere, chlorine activation by heterogeneous reactions starts in early winter which can indirectly be detected

Atmos. Chem. Phys. Discuss., https://doi.org/10.5194/acp-2018-202
Manuscript under review for journal Atmos. Chem. Phys.
Discussion started: 28 February 2018

Atmospheric Chemistry and Physics Discussions

by a depletion of the observed HCl mixing ratios. Wegner (2013) showed that in the dark core of the polar vortex, the observed depletion of HCl is much faster than in simulations of the Whole Atmosphere Community Climate Model (WACCM). This discrepancy, hereafter referred to as “HCl discrepancy", is documented in this paper and investigated in detail employing several well-established models, (1) the Lagrangian chemistry transport model CLaMS (Grooß et al., 2014), (2) WACCM (Marsh et al., 2013) and (3) TOMCAT/SLIMCAT (Chipperfield, 2006). The models CLaMS, WACCM and TOMCAT/SLIMCAT are described briefly in Section 2. The used observations are satellite data by the Microwave Limb Sounder (MLS) (Froidevaux et al., 2008) and the Michelson Interferometer for Passive Atmospheric Sounding (MIPAS) (Höpfner et al., 2007), which are described in Section 3. The model results and the comparison with the observations are shown in Section 4. The discussion in Sections 5 and 6 shows the characteristics of the likely missing process in the model and some hypotheses about which process could resolve the HCl discrepancy. Also, we quantify to what extent a potential additional chlorine activation mechanism would impact polar ozone loss.

2 Model description

2.1 CLaMS

The Chemical Lagrangian Model of the Stratosphere (CLaMS) is the main tool used here for the standard simulations and sensitivity tests. CLaMS is a Lagrangian chemistry-transport model that is described elsewhere (McKenna et al., 2002a, b; Grooß et al., 2014, and references therein). The model grid points are air parcels that follow trajectories and are therefore distributed irregularly in space. Also PSC particles are simulated along individual trajectories including also their gravitational settling. While in the study by Grooß et al. (2014) the Lagrangian PSC particle sedimentation scheme only simulates NAT particles, we include here an update that also simulates ice particles as described by Tritscher et al. (2018). Recent developments include the replacement of the previous chemistry solver routine IMPACT by a Newton-Raphson method derived from Wild and Prather (2000) as described by Morgenstern et al. (2009).

The model setup is very similar to that of Grooß et al. (2014). Initialisation and boundary conditions are derived from MLS observations of O_3, N_2O, H_2O, and HCl. The tropospheric domain is derived from a multi-annual simulation of CLaMS (Pommrich et al., 2014). Specific tracer-tracer correlations are used to derive the remaining chemical species. The simulation has 32 vertical levels below 900 K potential temperature with a vertical resolution of about 900 m in the lower stratosphere and a horizontal resolution of 100 km. The time span of the simulation is from 1 May 2011 until 31 October 2011. This year was chosen because both MIPAS and MLS data were available. Also shown for comparison are simulations with the same setup for the Arctic winter 2015/2016 starting at 1 November 2015 until 31 March 2016. However, we focus mainly on the Antarctic case.

Atmos. Chem. Phys. Discuss., https://doi.org/10.5194/acp-2018-202
Manuscript under review for journal Atmos. Chem. Phys.
Discussion started: 28 February 2018

Atmospheric Chemistry and Physics Discussions

2.2 WACCM

The Community Earth System Model version 1 (CESM1), Whole Atmosphere Community Climate Model (WACCM), is a coupled chemistry climate model from the Earth's surface to the lower thermosphere (Garcia et al., 2007; Kinnison et al., 2007; Marsh et al., 2013). WACCM is superset of the Community Atmosphere Model, version 4 (CAM4), and includes all of the physical parameterisations of CAM4 (Neale et al., 2013) and a finite volume dynamical core (Lin, 2004) for the tracer advection. The horizontal resolution is 1.9° latitude × 2.5° longitude and has 88 vertical levels up to about 150 km. The vertical resolution in the lower stratosphere ranges from 1.2 km near the tropopause to about 2 km near the stratopause; in the mesosphere and thermosphere the vertical resolution is about 3 km. For this work, the specified dynamics (SD) option is used (Lamarque et al., 2012). Here, temperature, zonal and meridional winds, and surface pressure are used to drive the physical parameterisation that control boundary layer exchanges, advective and convective transport, and the hydrological cycle. The meteorological analyses are taken from the National Aeronautics and Space Administration (NASA) Global Modeling and Assimilation Office (GMAO) Modern-Era Retrospective Analysis for Research and Applications (MERRA) (Rienecker et al., 2011) and the nudging approach is described by Kunz et al. (2011). The simulation used in the work is based on the International Global Atmospheric Chemistry / Stratosphere-troposphere Processes And their role in Climate (IGAC/SPARC) Chemistry Climate Model Initiative (CCMI) (Morgenstern et al., 2017). CESM1 (WACCM) includes a detailed representation of the chemical and physical processes in the troposphere through the lower thermosphere. The species included within this mechanism are contained within the O_x, NO_x, HO_x, ClO_x, and BrO_x chemical families, along with CH_4 and its degradation products. In addition, 20 primary non-methane hydrocarbons and related oxygenated organic compounds are represented along with their surface emissions. There is a total of 183 species and 472 chemical reactions; this includes 17 heterogeneous reactions on multiple aerosol types (i.e., sulphate, nitric acid trihydrate, and water-ice). Details on the stratospheric heterogeneous chemistry can be found in Wegner et al. (2013) and Solomon et al. (2015).

2.3 TOMCAT/SLIMCAT

TOMCAT/SLIMCAT (Chipperfield, 2006) is a gridpoint, Eulerian off-line 3-D chemical transport model which has been widely used for simulations of stratospheric chemistry (e.g. Dhomse et al., 2016; Chipperfield et al., 2017). Tracer transport is performed using the conservation of second-order moments scheme of Prather (1986). The model has a detailed description of stratospheric chemistry including reactions of the oxygen, nitrogen, hydrogen, chlorine and bromine families. Heterogeneous chemistry is treated on sulphate aerosols as well as liquid and solid PSCs. The model has a simple equilibrium scheme for the formation of nitric acid trihydrate particles, with an assumed supersaturation factor of 10 (Feng et al., 2011). The model chemistry is forced by specifying the time-dependent global mean values of source gases at the surface.

The model has a variable horizontal and vertical resolution. The model longitudes are regularly spaced while the latitude spacing can vary. Typically, the model is run using standard Gaussian grids associated with certain spectral resolutions. For the simulations presented here the model used either a 2.8°×2.8° resolution (T42 Gaussian grid) or a 1.2°×1.2° (T106 Gaussian grid) resolution. When forced by ECMWF analyses (as here) the model reads 6-hourly analyses of temperature, vorticity,

divergence, humidity and surface pressure as spectral coefficients. These quantities are averaged onto the model grid by spectral transforms. For both resolution experiments used here, ECMWF data at T42 resolution was used. The 6-hourly gridpoint meteorological fields are interpolated linearly in time. Near the pole the model groups gridboxes for transport in the east-west direction so that the tracer transport remains stable, which effectively degrades the resolution somewhat. In the runs used here vertical motion was calculated from the large-scale mass flux divergence on the model grid. The model used 32 hybrid sigma-pressure levels from the surface to about 60 km, with a resolution of 1.5-2.0 km in the lower stratosphere.

For the runs presented here the low resolution ($2.8° \times 2.8°$) simulation was initialised in 1977 and fully spun-up for the simulation of 2011. From 1989 the simulation was forced by ERA-Interim reanalyses. For the $1.2° \times 1.2°$ resolution simulation output from the low resolution simulation was interpolated to the higher resolution grid on January 1st, 2011 and the model integrated for 1 year. The use of pressure levels in the lower stratosphere can enhance the effects of numerical diffusion compared to theta levels (Chipperfield et al., 1997).

3 Data description

3.1 MLS data

The HCl observations by the Microwave Limb Sounder (MLS) on board the Aura satellite are the main data set used in this study (Froidevaux et al., 2008). MLS observes in limb viewing geometry on the so-called A-train orbit, cycling the earth 15 times daily covering latitudes from 82°S to 82°N. We use MLS version 4.2 data (Livesey et al., 2017). The vertical resolution in the lower stratosphere is about 3 km. The accuracy of HCl observations in the lower stratosphere is about 0.2 ppbv. The MLS observations of O_3, N_2O, and H_2O have also been used to constrain the CLaMS model initialisation and boundary condition.

3.2 MIPAS data

In addition to the MLS data, we also use data from the Michelson Interferometer for Passive Atmospheric Sounding (MIPAS) on Envisat. MIPAS operated between 2002 and 2012 and observed in limb geometry daily on about 15 orbits spanning the latitude range from 87°S to 89°N. In particular, $ClONO_2$ mixing ratios employing the KIT retrieval in the version V5R_CLONO2_221 have been used here. The vertical resolution in the lower stratosphere is about 3-4 km and the accuracy of the $ClONO_2$ observations is about 0.05 ppbv derived from correlative measurements (Höpfner et al., 2007). Unfortunately, it is difficult to retrieve the gas-phase mixing ratios from the infrared spectra in the presence of PSCs due to optical interference. Therefore, data gaps are unfortunately often present in the cold Antarctic stratosphere.

3.3 PSC detection by MIPAS and CALIOP

The possibility to detect PSCs from satellite measurements was also utilised in this study. We use the retrieval of PSCs from the infrared spectra of the MIPAS experiment on the Envisat satellite (Spang et al., 2016). The detection of PSCs from space-borne Cloud-Aerosol Lidar with Orthogonal Polarization (CALIOP) on the CALIPSO satellite was also used (Pitts et al., 2013).

Atmos. Chem. Phys. Discuss., https://doi.org/10.5194/acp-2018-202
Manuscript under review for journal Atmos. Chem. Phys.
Discussion started: 28 February 2018

Atmospheric Chemistry and Physics Discussions

CALIOP daily observes 15 orbits reaching latitudes of up to 82°in both hemispheres. It is possible to distinguish between the characteristics of different PSC types (STS, NAT, ice) from both instruments. Here we use only the detection of any PSCs, since the different PSC types are often coincident and the PSC type that dominates the optical signal may not be the relevant type here.

4 Development of HCl in polar stratosphere winter

The development of HCl in polar stratosphere winter is strongly influenced by the heterogeneous chlorine activation reactions. These reactions typically occur below a temperature threshold of about 195 K on cold binary aerosol or on PSCs that are either composed of super-cooled liquid ternary $HNO_3/H_2SO_4/H_2O$ solution (STS), water ice or crystalline nitric acid trihydrate (NAT). An important and fast HCl sink is the heterogeneous reaction

$$ClONO_2 + HCl \rightarrow HNO_3 + Cl_2.$$

At the beginning of the winter as temperatures decrease below the threshold for heterogeneous reactions to occur, this reaction quickly depletes HCl typically until all available $ClONO_2$ has reacted with HCl, since HCl is typically available in large excess. This step is therefore referred to as the "titration step". After that, HCl would stay constant in the dark without transport or mixing processes, since no reaction partner for HCl would be available. A further depletion of HCl is only possible, if there is a reaction partner that needs to be formed first, which could either be $ClONO_2$ or HOCl that would then react by the heterogeneous reaction

$$HOCl + HCl \rightarrow H_2O + Cl_2.$$

The resulting geographic distribution HCl and its development over the winter is presented in Figure 1. It shows maps of MLS HCl observations (Froidevaux et al., 2008) and corresponding CLaMS results on the 500 K potential temperature level for selected days on three consecutive months. On 21 May when the HCl depletion due to heterogeneous processing is first apparent, the model seems to represent the observations quite well. On 20 June, HCl depletion has mainly occurred at the vortex edge, where it is more distinctly pronounced in the observations. The comparison on 20 July clearly demonstrates the discrepancy between simulations and observations. The model shows still HCl mixing ratios well above 1.5 ppbv in the vortex core, while the MLS observations of HCl are almost completely zero within the limits of the total estimated uncertainty of the data.

To further investigate the HCl discrepancy, both the simulations and the data for each day were averaged with respect to equivalent latitude (Butchart and Remsberg, 1986) and potential temperature using 20 equivalent latitude (Φ_e) bins of equal area between Φ_e=50°S and 90°S. Figure 2 shows the characteristics of the observed HCl development by displaying cuts through the equivalent latitude/potential temperature space. The top left panel shows the time development of the vortex core average (Φ_e >75°S) as a function of potential temperature. The top right panel shows the time development on the 500 K potential temperature level. Grey lines correspond to the position of the cuts or borders displayed in the other panels. The bottom two panels show the Φ_e/θ cross sections for two selected days, here 20 June and 20 July. Figure 3 shows the corresponding results

Atmos. Chem. Phys. Discuss., https://doi.org/10.5194/acp-2018-202
Manuscript under review for journal Atmos. Chem. Phys.
Discussion started: 28 February 2018

from the CLaMS simulation. The top panels of Figs. 2 and 3 agree well with respect to the time at which the HCl depletion starts at the different altitudes and latitudes. However, it appears that after the first "titration" step, HCl depletes much slower in the simulations as opposed to the MLS observations. From the comparison of Figs. 2 and 3 it is evident, that the model HCl discrepancy is present over a wide altitude range throughout polar winter.

Figure 4 shows the time-series of the similarly averaged HCl mixing ratio for the Arctic winter 2015/2016, both for the MLS observations (top panels) and the CLaMS simulation (bottom panels). This winter was chosen, because it was particularly cold in the stratosphere (Dörnbrack et al., 2017). Here, the HCl discrepancy is also apparent, although to a lesser extent than in the Antarctic. It is most evident at somewhat lower potential temperature of about 475 K in the Arctic vortex core. Compared with the observations, the model needs over one month longer, until February, to reach the minimum HCl mixing ratios. In the following we focus however on the Antarctic results as the discrepancy is much more strongly pronounced.

The HCl discrepancy is also present in other models, for example Wohltmann et al. (2017) also mention a discrepancy in the vortex-average comparison of HCl observations with the Lagrangian model ATLAS, which has a very similar formulation to CLaMS (Wohltmann et al., 2010). However, they did not find an explanation for the discrepancy and thus they used an empirical correction to resolve the discrepancy, in which they apply a -5 K bias within the calculation of the HCl uptake into liquid particles, but without any further evidence of why that could be. For comparison, we also show here results for the Antarctic winter 2011 simulated by the global 3-D models WACCM and TOMCAT/SLIMCAT. Figure 5 shows the simulated HCl mixing ratios by WACCM and TOMCAT/SLIMCAT plotted identically as shown in Fig. 1. The HCl discrepancy is clearly also evident in these simulations, as both Eulerian models also show an area of elevated HCl in the polar vortex core still present on 20 July, when HCl had dissapeared in the MLS data, although with lower HCl mixing ratios compared to CLaMS. In the simulation by TOMCAT/SLIMCAT, the HCl depletion in the vortex core is stronger than in WACCM, but still not comparable to the MLS observations. For a more detailed comparison, the results of WACCM and TOMCAT/SLIMCAT have been averaged in Φ_e/θ space in a similar manner to CLaMS and the observations. The WACCM model daily output interpolated to potential temperature levels was averaged using potential vorticity and equivalent latitude provided from ERA-Interim data. The TOMCAT/SLIMCAT model output was directly averaged within the internal calculated equivalent latitude, also based on ERA-Interim data. A depiction corresponding to Fig. 3 but for WACCM and TOMCAT/SLIMCAT is shown as Figs. S1-S3 in the Supplementary Material. Figure 6 shows a time-series of the vortex-core-average HCl and $ClONO_2$ simulated by the three models. The green line corresponds to the MLS and MIPAS observations for HCl and $ClONO_2$, respectively. Unfortunately, only limited $ClONO_2$ observations are available from June to August, since the presence of PSCs impede the MIPAS retrieval process. There are differences between the individual models that arise due to different model formulation and initialisation and that are discussed below. Generally, the Eulerian models WACCM and TOMCAT/SLIMCAT show a faster HCl depletion than CLaMS. However it seems that all models under-estimate the rate of HCl depletion after the titration step.

All simulations show that the initial titration step is completed by the end of May and no strong changes of HCl until early July. Differences during May are likely caused by different initial chlorine partitioning. In July and August, HCl decreases further, where CLaMS is the model that indicates the slowest HCl decrease. There is even an apparent HCl increase in CLaMS, that is caused by the descent of airmasses with higher total chlorine Cl_y.

Atmos. Chem. Phys. Discuss., https://doi.org/10.5194/acp-2018-202
Manuscript under review for journal Atmos. Chem. Phys.
Discussion started: 28 February 2018

One possible reason for the inter-model difference could be differences in the chemistry formulation of the different models. To investigate this hypothesis, box model versions of TOMCAT/SLIMCAT and CLaMS were integrated along an example trajectory. This trajectory was chosen from an ensemble of 1800 vortex trajectories of 2.5 months length, along which the ozone and HCl development was closest to the vortex core average shown in Fig. 6. For this example trajectory, no significant differences were found between the models. Both models similarly showed no further depletion of HCl after the titration step in the dark, unmixed polar night conditions (see Fig. S4 of the Supplementary Material). Thus the difference among the models is likely not due to a difference in the formulation of the chemistry.

A large part of the the inter-model difference may be caused by the fact that the Lagrangian formulation of the model CLaMS minimises numerical diffusion while it is inherent in the Eulerian models WACCM and TOMCAT/SLIMCAT. The numerical diffusion arises in Eulerian models because on each time-step the chemical tracers are typically averaged within the extent of a model grid box. The minimisation of the numerical diffusion from this limit enhancing this lower resolution limit depends on the performance of the advection scheme, for example the Prather (1986) scheme used in TOMCAT/SLIMCAT stores sub-gridscale distributions of the tracers. The artificial mixing by numerical diffusion could provide additional $ClONO_2$ or HOCl as a reaction partner for HCl or NO_x that would form $ClONO_2$. To investigate this hypothesis, a sensitivity simulation by CLaMS was performed, in which a regular Eulerian grid with $2.8^\circ \times 2.8^\circ$ horizontal spacing and the vertical model grid (with the vertical resolution of 800-1000 m in the lower statosphere) as vertical levels were defined. Every 24 h of the model run it was checked, whether more than one air parcel resides in the same grid box. These air parcels were then set to the average mixing ratio of all air parcels residing in the grid box. Although an Eulerian model that must average over these grid boxes on every time-step would be even more diffusive, this study can at least show a lower limit of this effect. The corresponding HCl result (labelled “mix-Euler") is shown as orange line in Fig. 6. Indeed, the additional imposed Eulerian mixing causes a faster HCl depletion until mid-August. Although it is difficult to mimic additional numerical diffusion in a Lagrangian model, this sensitivity supports the assumption that at least part of the difference between CLaMS and the other Eulerian models maybe caused by numerical diffusion. Thus it is likely, that the numerical diffusion in the Eulerian models masks part of the effect responsible for the HCl discrepancy investigated in this study. However, there is not much difference in the development of HCl between the two resolutions of TOMCAT/SLIMCAT. In the low resolution simulation, the gradients of ozone and other trace species, especially at the vortex edge are smaller, but the time series of vortex core averages are very similar. Potentially, also in the high resolution simulation the numerical diffusion is already significant.

5 Characteristics of the HCl discrepancy

To find out more about the characteristics of the potentially missing process that could explain the difference between simulated and observed HCl in the core of the polar vortex, the comparison between simulations and observations were investigated especially for the vortex core data points on the 500 K level for 20 June (data from about 300 MLS profiles). This is a time and location, when both in the model and in the observations, the HCl depletion after the initial titration step is ongoing.

Atmos. Chem. Phys. Discuss., https://doi.org/10.5194/acp-2018-202
Manuscript under review for journal Atmos. Chem. Phys.
Discussion started: 28 February 2018

Atmospheric Chemistry and Physics Discussions

First, it is investigated, whether the missing process is correlated with temperature. This would be the case, if the depletion of HCl is caused by uptake on PSC particles, e.g. into the available liquid PSC particles as for example suggested by the empirical correction in Wohltmann et al. (2017). Similar to HNO_3, HCl is soluble in liquid aerosols. The solubility of HCl in the liquid aerosols given by the parametrisation of Carslaw et al. (1995) is included in the CLaMS chemistry module. Although the simulations do not show a significant HCl uptake, it may be, that underlying parameters like the Henry's law constant could be not accurately represented in the parametrisation. The uptake of HCl into the liquid aerosol particles should be strongly temperature-dependent (Carslaw et al., 1994) with the largest expected effect for the lowest temperatures. To examine such a hypothesis, the chosen subset of MLS data points and corresponding CLaMS points are plotted as function of temperature in Fig. 7. The temperature for all data points in this subset is below 194 K suggesting that PSCs should exist at the shown observation locations which is supported by the MIPAS PSC data base (Spang et al., 2017). Simulations and observations in Fig. 6 suggest that the first titration step is completed by 20 June. The temperature dependence of the difference between observations and the simulation is however not suggesting a missing uptake of HCl into the particles. Largest discrepancies between simulations and observations are found for higher temperatures. Therefore, the uptake of a significant fraction of HCl into the PSC particles seems to be an unlikely explanation for the shown discrepancy between Figs. 2 and 3.

Although the HCl depletion is not directly correlated with temperature, it seems likely that the missing process should require temperatures low enough for heterogeneous chlorine activation on PSCs or cold aerosols. In the following, we investigate whether the missing process requires sunlight. Therefore we investigated the history of the same observed air masses using 30-day back-trajectories calculated by the CLaMS trajectory module. From the trajectories, it was determined, how long the air-mass experienced sunlight and also how long they were exposed to temperatures below 195 K, a typical value below which PSCs can form and heterogeneous chemistry becomes important. Figure 8 shows the individual observed HCl mixing ratios as a function of the time spent at sunlight and below 195 K as green symbols. Red symbols show the corresponding simulated HCl mixing ratios. There seems to be a clear anti-correlation between the time spent in sunlight below 195 K and and HCl mixing ratios. This suggests that the missing process both requires sunlight and low temperatures as within the presence of PSCs.

To further clarify the temporal development of the HCl discrepancy, Fig. 9 shows also the rate of HCl change dHCl/dt calculated from the time series of HCl within the grid box in the equivalent latitude/potential temperature space for each day (middle panel). It is evident, that the first titration step caused by the heterogeneous reaction of HCl with $ClONO_2$ is reproduced correctly in the simulation. After that step, HCl decreases particularly strongly during two periods in mid-June and mid-July. These periods are correlated with a high occurrence fraction of PSCs as it is shown in the bottom panel of Fig. 9. The PSC occurrence fraction is shown for both MIPAS and CALIOP observations which are broadly consistent for the overlapping observation times. The only significant difference between MIPAS and CALIOP is in late May where MIPAS detects a large fraction of potentially small STS particles that could not be detected by CALIOP. Also in the beginning, these STS detections are pole-centered and therefore partly missed by the limited latitudinal coverage of the CALIPSO satellite. The anti-correlation between dHCl/dt and the PSC occurrence fraction is a further indication that PSCs may be relevant here. Possible processes missing in the formulation of the model that could explain the HCl discrepancy are investigated in the following sections.

Atmos. Chem. Phys. Discuss., https://doi.org/10.5194/acp-2018-202
Manuscript under review for journal Atmos. Chem. Phys.
Discussion started: 28 February 2018

6 Potential causes for the HCl discrepancy

The required missing process, or a set of missing processes, should improve the characteristic difference between observed and simulated HCl mixing ratios (Figs. 2 and 3). By incorporating different processes into a model we investigate the "fingerprint" of the corresponding change to the model results. This method will not provide a proof of whether a hypothetical process occurs in reality. However, it can help to exclude hypothetical processes when they cause different "fingerprints" that can be contrasted with observations. In the following subsections, different hypotheses for the missing processes are investigated by incorporation into the model CLaMS.

6.1 Ionisation from galactic cosmic rays

One well-known process that is often neglected in simulations of stratospheric chemistry is the ionisation of air molecules by galactic cosmic rays. Galactic cosmic rays would provide an additional source of NO_x and HO_x (Warneck, 1972; Rusch et al., 1981; Solomon et al., 1981; Müller and Crutzen, 1993). An additional source of OH and NO in the polar stratosphere triggers an HCl sink through the following reaction chains:

$$\begin{aligned} NO + O_3 &\rightarrow NO_2 + O_2 \\ NO_2 + ClO &\xrightarrow{M} ClONO_2 \\ HCl + ClONO_2 &\xrightarrow{het} Cl_2 + HNO_3 \end{aligned}$$

and

$$\begin{aligned} OH + O_3 &\rightarrow HO_2 + O_2 \\ HO_2 + ClO &\rightarrow HOCl + O_2 \\ HOCl + HCl &\xrightarrow{het} Cl_2 + H_2O \end{aligned}$$

These reaction chains are only effective in the presence of heterogeneously active particle surfaces (cold binary aerosols or PSCs) and in the presence of sunlight since the ClO molecule would be converted into Cl_2O_2 in darkness. To investigate this effect, the NO_x and HO_x sources from cosmic-ray induced ionisation pair were incorporated into the chemistry module of CLaMS. The ionisation rate was induced after Heaps (1978) using the efficiency $\mathrm{eff}_{\mathrm{NO}}$=1.25 and $\mathrm{eff}_{\mathrm{HOx}}$=2 for the formation of NO and OH per ionisation, respectively (Jackman et al., 2016). Fig. 10 shows the corresponding vortex core average (Φ_e >75°S) on the 500 K level for the reference simulation and the simulation including induced ionisation by the galactic cosmic rays (GCR). Indeed, such an ionisation rate to the model does introduce an accelerated HCl decomposition in the polar vortex where active chlorine exists. However, the effect is too small to explain the CLaMS HCl discrepancy shown in Section 4. By early August, the HCl discrepancy shown here is reduced by about 20%. Even though there are newer estimates of the GCR-induced ionisation rate (Usoskin et al., 2010; Jackman et al., 2016), they are not significantly larger so a severe under-estimation of the GCR-induced ionisation rate seems unlikely.

Atmos. Chem. Phys. Discuss., https://doi.org/10.5194/acp-2018-202
Manuscript under review for journal Atmos. Chem. Phys.
Discussion started: 28 February 2018

6.2 Photolysis of particulate HNO_3

Besides the photolysis of gas-phase HNO_3, it may be possible that also the HNO_3 bound in PSC particles photolyses directly. Evidenc for this comes from studies which have shown that nitrate photolysis from snow surfaces is a significant source of NO_x at the Earth's surface (e.g. Honrath et al., 1999; Dominé and Shepson, 2002) and that nitrate photolysis in the quasi-liquid layer in laboratory surface studies is enhanced in the presence of halide ions due to a reduced solvent cage effect (Wingen et al., 2008; Richards et al., 2011). These studies suggest that photolysis of dissolved HNO_3 in PSC particles, including STS droplets, may be possible. If such a process could liberate NO_x or HO_x into the gas phase from the particle phase, it could also cause HCl depletion by the reaction chains mentioned above. However, we note that such a process is yet unproven. Wegner (2013) investigated this hypothesis by implementing this process into the model WACCM. He used the cross-section for the NO_3^- ion (Chu and Anastasio, 2003), with a quantum yield of 0.3 reflecting relatively high values seen on some surfaces in laboratory experiments (Abida et al., 2012). These simulations indicated that due to the low solar elevation in austral winters, the onset of HCl depletion in June cannot be reproduced by adding this process. Furthermore, this NO_x-source would cause an over-estimation of $ClONO_2$ at higher solar elevation in September.

Here we extend this investigation by Wegner (2013) by including possible upper and lower limits for this process, as the photolysis of particulate HNO_3 on PSCs has not been investigated in detail. Laboratory measurements show that combined absorption cross sections of HNO_3(aq) and NO_3 in bulk solutions are significantly larger than those in the gas phase (Chu and Anastasio, 2003; Svoboda et al., 2013). Quantum yields in the aqueous bulk phase are small, $\approx$1% or less (Warneck and Wurzinger, 1988; Benedict et al., 2017). However, quantum yield on surfaces may be much larger (Abida et al., 2012), and such large quantum yields are also suggested by strong NO_x-emissions from nitrate-containing particles exposed to UV radiation (Reed et al., 2017; Ye et al., 2016; Baergen and Donaldson, 2013). As a lower limit for the photolysis of particulate HNO_3 we apply also the gas phase photolysis of HNO_3 to the NAT particles with a quantum yield of 1. As an estimate for the upper limit, we use observations of the absorption cross sections in ice by Chu and Anastasio (2003) and also a quantum yield of 1. The used absorption cross sections and the photolysis rates derived from that are shown in Fig. S5 of the Supplementary Material. As in Fig. 10, Figure 11 shows the HCl and $ClONO_2$ data, the CLaMS GCR simulation (blue) and the upper and lower limit as described above. The lower limit (blue lines) is not much different from the CLaMS simulation without this process. In the simulation for the upper limit, an additional faster depletion of HCl is clearly visible. However, throughout the month of June, the effect is not large enough to fully explain the remaining HCl discrepancy. Furthermore, the simulation indicates that this process would significantly enhance the chlorine deactivation into $ClONO_2$ in late August and September. Therefore, the upper limit simulation appears not to be the process that would resolve the HCl discrepancy. Potentially, this process with a lower quantum yield may explain the small discrepancy in $ClONO_2$ in September. The fingerprint of a photolysis-like process increases with solar elevation and therefore would be much stronger in September than in June. However, there may be a similar processes independent of sunlight that could decompose condensed-phase HNO_3 as discussed in the following section.

Atmos. Chem. Phys. Discuss., https://doi.org/10.5194/acp-2018-202
Manuscript under review for journal Atmos. Chem. Phys.
Discussion started: 28 February 2018

Atmospheric Chemistry and Physics Discussions

6.3 Decomposition of particulate HNO_3

A similar hypothesis to that described in the previous section would be the decomposition of the condensed-phase HNO_3 by a process other than photolysis. A more steady decomposition throughout the polar winter could be triggered, for example, by galactic cosmic rays (GCRs) instead of by photolysis. Especially over the poles, secondary electrons from GCRs that do not have enough energy to decompose air molecules may still be able to interact with HNO_3 on the PSCs. In Fig. 12, the HCl discrepancy in June and July steadily increases with time in the presence of NAT or ice PSCs. To achieve the observed HCl depletion rate on the 500 K potential temperature level, about 1% of the condensed HNO_3 per day needs to be liberated into the gas phase. The exact mechanism, how this could work needs to be clarified, but to investigate the impact of this hypothesis, we performed a test simulation in which the HNO_3 on NAT is decomposed into NO_2+OH at a constant rate of $10^{-7}s^{-1}$ independent of altitude (labelled “NAT decomp").

Figure 12 shows the simulated HCl mixing ratios in Φ_e/θ-space. Even though not every detail of the observations is reproduced, it is evident, that this simulation significantly better describes the observations than any of the hypotheses discussed above. The rate of the hypothetical process was chosen such that the HCl depletion on the 500 K level is well represented. It is evident that above this level, this rate should be increasing, however, it does not seem appropriate here to speculate further.

One further piece of evidence for the hypothesis that a possible NO_x-source from PSC decomposition exists is given by the comparison with $ClONO_2$ data. Figure 12 shows the time development of vortex core mixing ratios of HCl and $ClONO_2$ on the 500 K potential temperature level. The blue line in the top panel demonstrates that on this level the observed HCl depletion is represented by the simulation “NAT decomp". The MIPAS observations of $ClONO_2$ are intermittent since a lot of observations are blocked by the presence of PSCs. However, the remaining observations indicate low mixing ratios in the range between 0.05 and 0.1 ppbv between late May and late August. This observation is also better reproduced by the simulation “NAT decomp" than both other simulations in which $ClONO_2$ is nearly zero between early June and end of September.

The complete fingerprint of the 3-dimensional HCl development similar to Figs. 2 and 3 is shown in Fig. 13. Although differences remain, this sensitivity experiment simulates the HCl observations much better than any other CLaMS simulations discussed here.

6.4 Impact on polar ozone depletion

The potential process that was included in the simulation "NAT decomp" increases chlorine activation significantly, especially in the polar winter. This might be expected to also affect the simulated ozone depletion. However, the difference in chlorine activation is especially large in the rather dark vortex core, where chemical ozone depletion rates are small. Therefore, we also investigated the impact of the hypothetical NAT decomposition processes on polar ozone depletion. Figure 14 shows the simulated chemical ozone depletion for the three simulations, the reference simulation, the simulation including GCR-induced ionisation and the simulation including also the hypothetical NAT decomposition. The ozone depletion is also shown for the simulation for the Arctic winter 2015/2016 employing the same model sensitivities. Although it is clear that an increase in chlorine activation yields more ozone depletion, the overall effect on ozone depletion of this additional hypothetical process is

rather low. The increase of column ozone loss due to GCR-induced ionisation ranges from 2% to 3%. The additional column ozone loss due to the hypothetical NAT decomposition is calculated to be about 1.8%.

7 Conclusions

In this paper we have demonstrated that an important polar wintertime process which leads to the removal of HCl is missing in the standard formulation of stratospheric chemistry. The discrepancy between observed and simulated abundances of HCl is apparent in the dark polar vortex cores in stratospheric winter. In the simulations, there is little change in HCl after the first titration step through the heterogeneous reaction of HCl with $ClONO_2$. In contrast, the observations show a continuous removal of HCl from the gas phase even in the dark core of the polar vortex. This discrepancy is somewhat masked in Eulerian global models due to the inherent numerical diffusion.

A detailed investigation of the characteristics of the HCl discrepancy points to a further missing process that likely involves PSCs. Several hypotheses of the cause of the discrepancy have been investigated. The incorporation of GCR induced ionisation reduces the discrepancy somewhat, but is by far not sufficient. The uptake of HCl into PSC particles and photolysis of particulate HNO_3 also cannot explain the HCl discrepancy. Simulations with a hypothetical steady decomposition of HNO_3 out of NAT PSCs would be suited to resolve the HCl discrepancy. This may be caused indirectly by GCRs. At least, the observation of a small increase in $ClONO_2$ suggests the presence of an additional NO_x source. The exact process responsible for the HCl decomposition remains the subject of further research. Since the discrepancy occurs during the beginning of the chlorine activation period in winter where the ozone loss rates are slow, there is only a minor impact on the overall ozone loss in polar spring.

Acknowledgements. The authors gratefully acknowledge the computing time for the CLaMS simulations granted on the supercomputer JURECA at Jülich Supercomputing Centre (JSC) under the VSR project ID JICG11. The TOMCAT/SLIMCAT modelling work was supported by the NERC National Centre for Atmospheric Science (NCAS). The simulations were performed on the UK Archer and Leeds ARC HPC facilities. The National Center for Atmospheric Research (NCAR) is sponsored by the U.S. National Science Foundation (NSF). WACCM is a component of NCAR's Community Earth System Model (CESM), which is supported by the NSF and the Office of Science of the U.S. Department of Energy. Computing resources were provided by NCAR's Climate Simulation Laboratory, sponsored by NSF and other agencies. This research was enabled by the computational and storage resources of NCAR's Computational and Information Systems Laboratory (CISL). The model output and data used in this paper are listed in the references or available from the NCAR Earth System Grid. We also acknowledge the International Space Science Institute (ISSI) for supporting the Polar Stratospheric Cloud Initiative (PSCi). We are grateful to the European Centre for Medium-Range Weather Forecasts (ECMWF) for providing the meteorological re-analyses. Ines Tritscher was funded by the Deutsche Forschungsgemeinschaft (DFG) under project number 310479827. We thank Michelle Santee and the MLS team, Gabriele Stiller and the MIPAS-Envisat team for the enormous work on providing their high quality data sets. We also thank Susan Solomon and Michael Höpfner for fruitful discussions on aspects of this study.

References

Abida, O., Du, J., and Zhu, L.: Investigation of the photolysis of the surface-adsorbed HNO3 by combining laser photolysis with Brewster angle cavity ring-down spectroscopy, Chem. Phys. Lett., 534, 77–82, https://doi.org/10.1016/j.cplett.2012.03.034, 2012.

Baergen, A. M. and Donaldson, D. J.: Photochemical renoxification of nitric acid on real urban grime, Environ. Sci. Technol., 47, 815–820, https://doi.org/10.1021/es3037862, 2013.

Benedict, K. B., McFall, A. S., and Anastasio, C.: Quantum yield of nitrite from the photolysis of aqueous nitrate above 300 nm, Environ. Sci. Technol., 51, 4387–4395, https://doi.org/10.1021/acs.est.6b06370, 2017.

Butchart, N. and Remsberg, E. E.: The area of the stratospheric polar vortex as a diagnostic for tracer transport on an isentropic surface, J. Atmos. Sci., 43, 1319–1339, 1986.

Carslaw, K. S., Luo, B. P., Clegg, S. L., Peter, T., Brimblecombe, P., and Crutzen, P. J.: Stratospheric aerosol growth and HNO_3 gas phase depletion from coupled HNO_3 and water uptake by liquid particles, Geophys. Res. Lett., 21, 2479–2482, https://doi.org/10.1029/94GL02799, 1994.

Carslaw, K. S., Clegg, S. L., and Brimblecombe, P.: A thermodynamic model of the system HCl-HNO_3-H_2SO_4-H_2O, including solubilities of HBr, from 328 K to $<$ 200 K, J. Phys. Chem., 99, 11 557–11 574, 1995.

Chipperfield, M. P.: New version of the TOMCAT/SLIMCAT off-line chemical transport model: Intercomparison of stratospheric tracer experiments, Q. J. R. Meteorol. Soc., 132, https://doi.org/10.1256/qj.05.51, 2006.

Chipperfield, M. P., Lutman, E. R., Kettleborough, J. A., and Pyle, J. A.: Model studies of chlorine deactivation and formation of $ClONO_2$ collar in the Arctic polar vortex, J. Geophys. Res., 102, 1467–1478, 1997.

Chipperfield, M. P., Bekki, S., Dhomse, S., Harris, N. R. P., Hassler, B., Hossaini, R., Steinbrecht, W., Thieblemont, R., and Weber, M.: Detecting recovery of the stratospheric ozone layer, Nature, 549, 211–218, https://doi.org/10.1038/nature23681, 2017.

Chu, L. and Anastasio, C.: Quantum yields of hydroxyl radical and nitrogen dioxide from the photolysis of nitrate on ice, J. Phys. Chem. A, 107, 9594–9602, https://doi.org/10.1021/jp0349132, 2003.

Crutzen, P. J. and Arnold, F.: Nitric acid cloud formation in the cold Antarctic stratosphere: A major cause for the springtime 'ozone hole', Nature, 342, 651–655, 1986.

Dhomse, S. S., Chipperfield, M. P., Damadeo, R. P., Zawodny, J. M., Ball, W. T., Feng, W., Hossaini, R., Mann, G. W., and Haigh, J. D.: On the ambiguous nature of the 11 year solar cycle signal in upper stratospheric ozone, Geophys. Res. Lett., 43, 7241–7249, https://doi.org/10.1002/2016GL069958, 2016.

Dominé, F. and Shepson, P. B.: Air-snow interactions and atmospheric chemistry, Science, 297, 1506–1510, https://doi.org/10.1126/science.1074610, 2002.

Dörnbrack, A., Gisinger, S., Pitts, M. C., Poole, L. R., and Maturilli, M.: Multilevel Cloud Structures over Svalbard, Monthly Weather Review, 145, 1149–1159, https://doi.org/10.1175/MWR-D-16-0214.1, 2017.

Drdla, K. and Müller, R.: Temperature thresholds for chlorine activation and ozone loss in the polar stratosphere, Ann. Geophys., 30, 1055–1073, https://doi.org/10.5194/angeo-30-1-2012, 2012.

Fahey, D. W., Gao, R. S., Carslaw, K. S., Kettleborough, J., Popp, P. J., Northway, M. J., Holecek, J. C., Ciciora, S. C., McLaughlin, R. J., Thompson, T. L., Winkler, R. H., Baumgardner, D. G., Gandrud, B., Wennberg, P. O., Dhaniyala, S., McKinley, K., Peter, T., Salawitch, R. J., Bui, T. P., Elkins, J. W., Webster, C. R., Atlas, E. L., Jost, H., Wilson, J. C., Herman, R. L., Kleinböhl, A., and von König, M.: The detection of large HNO_3-containing particles in the winter Arctic stratosphere, Science, 291, 1026–1031, 2001.

Farman, J. C., Gardiner, B. G., and Shanklin, J. D.: Large losses of total ozone in Antarctica reveal seasonal ClO_x/NO_x interaction, Nature, 315, 207–210, 1985.

Feng, W., Chipperfield, M. P., Davies, S., Mann, G. W., Carslaw, K. S., Dhomse, S., Harvey, L., Randall, C., and Santee, M. L.: Modelling the effect of denitrification on polar ozone depletion for Arctic winter 2004/2005, Atmos. Chem. Phys., 11, 6559–6573, https://doi.org/10.5194/acp-11-6559-2011, 2011.

Froidevaux, L., Jiang, Y. B., Lambert, A., Livesey, N. J., Read, W. G., Waters, J. W., Fuller, R. A., Marcy, T. P., Popp, P. J., Gao, R. S., Fahey, D. W., Jucks, K. W., Stachnik, R. A., Toon, G. C., Christensen, L. E., Webster, C. R., Bernath, P. F., Boone, C. D., Walker, K. A., Pumphrey, H. C., Harwood, R. S., Manney, G. L., Schwartz, M. J., Daffer, W. H., Drouin, B. J., Cofield, R. E., Cuddy, D. T., Jarnot, R. F., Knosp, B. W., Perun, V. S., Snyder, W. V., Stek, P. C., Thurstans, R. P., and Wagner, P. A.: Validation of Aura Microwave Limb Sounder HCl measurements, J. Geophys. Res., 113, D15S25, https://doi.org/10.1029/2007JD009025, 2008.

Garcia, R. R., Marsh, D. R., Kinnison, D. E., Boville, B. A., and Sassi, F.: Simulation of secular trends in the middle atmosphere, 1950–2003, J. Geophys. Res., 112, D09301, https://doi.org/10.1029/2006JD007485, 2007.

Grooß, J.-U., Günther, G., Müller, R., Konopka, P., Bausch, S., Schlager, H., Voigt, C., Volk, C. M., and Toon, G. C.: Simulation of denitrification and ozone loss for the Arctic winter 2002/2003, Atmos. Chem. Phys., 5, 1437–1448, 2005.

Grooß, J.-U., Brautzsch, K., Pommrich, R., Solomon, S., and Müller, R.: Stratospheric ozone chemistry in the Antarctic: What controls the lowest values that can be reached and their recovery?, Atmos. Chem. Phys., 11, 12 217–12 226, 2011.

Grooß, J.-U., Engel, I., Borrmann, S., Frey, W., Günther, G., Hoyle, C. R., Kivi, R., Luo, B. P., Molleker, S., Peter, T., Pitts, M. C., Schlager, H., Stiller, G., Vömel, H., Walker, K. A., and Müller, R.: Nitric acid trihydrate nucleation and denitrification in the Arctic stratosphere, Atmos. Chem. Phys., 14, 1055–1073, https://doi.org/10.5194/acp-14-1055-2014, 2014.

Heaps, M. G.: Parametization of the cosmic ray ion-pair production rate above 18 km, Planet Space Sci., 26, 513–517, 1978.

Honrath, R. E., Peterson, M. C., Guo, S., Dibb, J. E., Shepson, P. B., and Campbell, B.: Evidence of NO_x production within or upon ice particles in the Greenland snowpack, Geophys. Res. Lett., 26, 695–698, https://doi.org/10.1029/1999GL900077, 1999.

Höpfner, M., von Clarmann, T., Fischer, H., Funke, B., Glatthor, N., Grabowski, U., Kellmann, S., Kiefer, M., Linden, A., Milz, M., Steck, T., Stiller, G. P., Bernath, P., Blom, C. E., Blumenstock, T., Boone, C., Chance, K., Coffey, M. T., Friedl-Vallon, F., Griffith, D., Hannigan, J. W., Hase, F., Jones, N., Jucks, K. W., Keim, C., Kleinert, A., Kouker, W., Liu, G. Y., Mahieu, E., Mellqvist, J., Mikuteit, S., Notholt, J., Oelhaf, H., Piesch, C., Reddmann, T., Ruhnke, R., Schneider, M., Strandberg, A., Toon, G., Walker, K. A., Warneke, T., Wetzel, G., Wood, S., and Zander, R.: Validation of MIPAS $ClONO_2$ measurements, Atmos. Chem. Phys., 7, 257–281, https://doi.org/10.5194/acp-7-257-2007, https://www.atmos-chem-phys.net/7/257/2007/, 2007.

Jackman, C. H., Marsh, D. R., Kinnison, D. E., Mertens, C. J., and Fleming, E. L.: Atmospheric changes caused by galactic cosmic rays over the period 1960–2010, Atmos. Chem. Phys., 16, 5853–5866, https://doi.org/10.5194/acp-16-5853-2016, 2016.

Kinnison, D. E., Brasseur, G. P., Walters, S., Garcia, R. R., Sassi, D. R. M. F., Harvey, V. L., Randall, C. E., Emmons, L., Lamarque, J. F., Hess, P., Orlando, J. J., Tie, X. X., Randel, W., Pan, L. L., Gettelman, A., Granier, C., Diehl, T., Niemeier, U., and Simmons, A. J.: Sensitivity of chemical tracers to meteorological parameters in the MOZART-3 chemical transport model, J. Geophys. Res., 112, https://doi.org/10.1029/2006JD007879, 2007.

Kunz, A., Pan, L. L., Konopka, P., Kinnison, D. E., and Tilmes, S.: Chemical and dynamical discontinuity at the extratropical tropopause based on START08 and WACCM analyses, J. Geophys. Res., 116, https://doi.org/10.1029/2011JD016686, 2011.

Lamarque, J. F., Emmons, L. K., Hess, P. G., Kinnison, D. E., Tilmes, S., Vitt, F., Heald, C. L., Holland, E. A., Lauritzen, P. H., Neu, J., Orlando, J. J., Rasch, P. J., and Tyndall, G. K.: CAM-chem: description and evaluation of interactive atmospheric chemistry in the Community Earth System Model, Geosci. Model Dev., 5, 369–411, https://doi.org/10.5194/gmd-5-369-2012, 2012.

Lin, S.: A "vertically Lagrangian" finite-volume dynamical core for global models, Monthly Weather Review, 132, 2293–2307, 2004.

Livesey, N. J., Read, W. G., Wagner, P. A., Froidevaux, L., Lambert, A., Manney, G. L., Valle, L. F. M., Pumphrey, H. C., Santee, M. L., Schwartz, M. J., Wang, S., Fuller, R. A., Jarnot, R. F., Knosp, B. W., and Martinez, E.: Version 4.2x Level 2 data quality and description document, JPL D-33509 Rev. C, https://mls.jpl.nasa.gov/data/v4-2_data_quality_document.pdf, 2017.

Marsh, D. R., Mills, M. J., Kinnison, D. E., LAmarque, J.-F., Calvo, N., and Polvani, L. M.: Climate change from 1850 to 2005 simulated in CESM1(WACCM), Journal of Climate, 26, 7372–7390, https://doi.org/10.1175/JCLI-D-12-00558.1, 2013.

McKenna, D. S., Konopka, P., Grooß, J.-U., Günther, G., Müller, R., Spang, R., Offermann, D., and Orsolini, Y.: A new Chemical Lagrangian Model of the Stratosphere (CLaMS): 1. Formulation of advection and mixing, J. Geophys. Res., 107, 4309, https://doi.org/10.1029/2000JD000114, 2002a.

McKenna, D. S., Grooß, J.-U., Günther, G., Konopka, P., Müller, R., Carver, G., and Sasano, Y.: A new Chemical Lagrangian Model of the Stratosphere (CLaMS): 2. Formulation of chemistry scheme and initialization, J. Geophys. Res., 107, 4256, https://doi.org/10.1029/2000JD000113, 2002b.

Molina, M. J. and Rowland, F. S.: Stratospheric sink for chlorofluoromethanes: chlorine atom-catalysed destruction of ozone, Nature, 249, 810–812, 1974.

Morgenstern, O., Braesicke, P., O'Connor, F. M., Bushell, A. C., Johnson, C. E., Osprey, S. M., and Pyle, J. A.: Evaluation of the new UKCA climate-composition model – Part 1: The stratosphere, Geosci. Model Dev., 2, 43–57, http://www.geosci-model-dev.net/2/43/2009/, 2009.

Morgenstern, O., Hegglin, M. I., Rozanov, E., O'Connor, F. M., Abraham, N. L., Akiyoshi, H., Archibald, A. T., Bekki, S., Butchart, N., Chipperfield, M. P., Deushi, M., Dhomse, S. S., Garcia, R. R., Hardiman, S. C., Horowitz, L. W., Joeckel, P., Josse, B., Kinnison, D., Lin, M., Mancini, E., Manyin, M. E., Marchand, M., Marecal, V., Michou, M., Oman, L. D., Pitari, G., Plummer, D. A., Revell, L. E., Saint-Martin, D., Schofield, R., Stenke, A., Stone, K., Sudo, K., Tanaka, T. Y., Tilmes, S., Yamashita, Y., Yoshida, K., and Zeng, G.: Review of the global models used within phase 1 of the Chemistry-Climate Model Initiative (CCMI), Geosci. Model Dev., 10, 639–671, https://doi.org/10.5194/gmd-10-639-2017, 2017.

Müller, R. and Crutzen, P. J.: A possible role of galactic cosmic rays in chlorine activation during polar night, J. Geophys. Res., 98, 20 483–20 490, 1993.

Müller, R., Grooß, J.-U., Zafar, A. M., and Lehmann, R.: The maintenance of elevated active chlorine levels in the Antarctic lower stratosphere through HCl null-cycles, Atmospheric Chemistry and Physics Discussions, pp. 1–20, https://doi.org/10.5194/acp-2017-833, https://www.atmos-chem-phys-discuss.net/acp-2017-833/, 2017.

Nash, E. R., Newman, P. A., Rosenfield, J. E., and Schoeberl, M. R.: An objective determination of the polar vortex using Ertel's potential vorticity, J. Geophys. Res., 101, 9471–9478, 1996.

Neale, R. B., Richter, J., Park, S., Lauritzen, P. H., Vavrus, S. J., Rasch, P. J., and Zhang, M.: The mean climate of the Community Atmosphere Model (CAM4) in forced SST and fully coupled experiments, J. Climate, 26, 5150–5168, https://doi.org/10.1175/JCLI-D-12-00236.1, 2013.

Peter, T.: Microphysics and heterogeneous chemistry of polar stratospheric clouds, Ann. Rev. Phys. Chem., 48, 785–822, 1997.

Pitts, M. C., Poole, L. R., Dörnbrack, A., and Thomason, L. W.: The 2009-2010 Arctic polar stratospheric cloud season: A CALIPSO perspective, Atmos. Chem. Phys., 11, 2161–2177, https://doi.org/10.5194/acp-11-2161-2011, 2011.

Pitts, M. C., Poole, L. R., Lambert, A., and Thomason, L. W.: An assessment of CALIOP polar stratospheric cloud composition classification, Atmos. Chem. Phys., 13, 2975–2988, https://doi.org/10.5194/acp-13-2975-2013, https://www.atmos-chem-phys.net/13/2975/2013/, 2013.

Pommrich, R., Müller, R., Grooß, J.-U., Konopka, P., Ploeger, F., Vogel, B., Tao, M., Hoppe, C. M., Günther, G., Spelten, N., Hoffmann, L., Pumphrey, H.-C., Viciani, S., D'Amato, F., Volk, C. M., Hoor, P., Schlager, H., and Riese, M.: Tropical troposphere to stratosphere transport of carbon monoxide and long-lived trace species in the Chemical Lagrangian Model of the Stratosphere (CLaMS), Geoscientific Model Development, 7, 2895–2916, https://doi.org/10.5194/gmd-7-2895-2014, http://www.geosci-model-dev.net/7/2895/2014/, 2014.

Prather, M. J.: Numerical advection by conservation of second-order moments, J. Geophys. Res., 91, 6671–6681, https://doi.org/10.1029/JD091iD06p06671, 1986.

Reed, C., Evans, M. J., Crilley, L. R., Bloss, W. J., Sherwen, T., Read, K. A., Lee, J. D., and Carpenter, L. J.: Evidence for renoxification in the tropical marine boundary layer, Atmos. Chem. Phys., 17, 4081–4092, https://doi.org/10.5194/acp-17-4081-2017, 2017.

Richards, N. K., Wingen, L.-M., Callahan, K. M., Nishino, N., Kleinman, M. T., Tobias, D. J., , and Finlayson-Pitts, B. J.: Nitrate ion photolysis in thin water films in the presence of bromide ions, J. Phys. Chem. A, 115, 5810–5821, https://doi.org/10.1021/jp109560, 2011.

Rienecker, M. M., Suarez, M. J., Gelaro, R., Todling, R., Bacmeister, J., Liu, E., Bosilovich, M. G., Schubert, S. D., Takacs, L., Kim, G.-K., Bloom, S., Chen, J., Collins, D., Conaty, A., Da Silva, A., Gu, W., Joiner, J., Koster, R. D., Lucchesi, R., Molod, A., Owens, T., Pawson, S., Pegion, P., Redder, C. R., Reichle, R., Robertson, F. R., Ruddick, A. G., Sienkiewicz, M., and Woollen, J.: MERRA: NASA's Modern-Era Retrospective Analysis for Research and Applications, J. Climate, 24, 3624–3648, https://doi.org/10.1175/JCLI-D-11-00015.1, 2011.

Rusch, D. W., Gerard, J. C., Solomon, S., Crutzen, P. J., and Reid, G. C.: The effect of particle precipitation events on the neutral and ion chemistry of the middle atmosphere: I. Odd nitrogen, Planet. Space Sci., 29, 767–774, 1981.

Schoeberl, M. R. and Hartmann, D. L.: The Dynamics of the Stratospheric Polar Vortex and Its Relation to Springtime Ozone Depletions, Science, 251, 46–52, 1991.

Shi, Q., Jayne, J. T., Kolb, C. E., Worsnop, D. R., and Davidovits, P.: Kinetic model for reaction of $ClONO_2$ with H_2O and HCl and HOCl with HCl in sulfuric acid solutions, J. Geophys. Res., 106, 24 259–24 274, https://doi.org/10.1029/2000JD000181, 2001.

Solomon, S.: Stratospheric ozone depletion: A review of concepts and history, Rev. Geophys., 37, 275–316, https://doi.org/10.1029/1999RG900008, 1999.

Solomon, S., Rusch, D. W., Gerard, J. C., Reid, G. C., and Crutzen, P. J.: The effect of particle precipitation events on the neutral and ion chemistry of the middle atmosphere: II. Odd hydrogen, Planet. Space Sci., 29, 885 – 892, 1981.

Solomon, S., Garcia, R. R., Rowland, F. S., and Wuebbles, D. J.: On the depletion of Antarctic ozone, Nature, 321, 755–758, 1986.

Solomon, S., Kinnison, D., Bandoro, J., and Garcia, R.: Simulation of polar ozone depletion: An update, J. Geophys. Res., 120, 7958–7974, https://doi.org/10.1002/2015JD023365, 2015.

Spang, R., Hoffmann, L., Höpfner, M., Griessbach, S., Müller, R., Pitts, M. C., Orr, A. M. W., and Riese, M.: A multi-wavelength classification method for polar stratospheric cloud types using infrared limb spectra, Atmos. Meas. Tech., 9, 3619–3639, https://doi.org/10.5194/amt-9-3619-2016, 2016.

Spang, R., Hoffmann, L., Müller, R., Grooß, J.-U., Tritscher, I., Höpfner, M., Pitts, M., Orr, A., and Riese, M.: A climatology of polar stratospheric cloud composition between 2002 and 2012 based on MIPAS/Envisat observations, Atmos. Chem. Phys. Discuss., pp. 1–44, https://doi.org/10.5194/acp-2017-898, https://www.atmos-chem-phys-discuss.net/acp-2017-898/, 2017.

Stolarski, R. S., Krueger, A. J., Schoeberl, M. R., McPeters, R. D., Newman, P. A., and Alpert, J. C.: Nimbus 7 satellite measurements of the springtime Antarctic ozone decrease, Nature, 322, 808–811, 1986.

Svoboda, O., Kubelova, L., and Slavicek, P.: Enabling forbidden processes: Quantum and solvation enhancement of nitrate anion UV absorption, J. Phys. Chem. A, 117, 12 868–12 877, https://doi.org/10.1021/jp4098777, 2013.

Tritscher, I., Grooß, J.-U., Spang, R., Pitts, M. P., Müller, R., and Riese, M.: Lagrangian simulation of ice particles in the polar winter stratosphere, Atmos. Chem. Phys., in preparation, 2018.

Usoskin, I. G., Kovaltsov, G. A., and Mironova, I. A.: Cosmic ray induced ionization model CRAC:CRII: An extension to the upper atmosphere, J. Geophys. Res., 115, https://doi.org/10.1029/2009JD013142, 2010.

Warneck, P.: Cosmic-radiation as a source of odd nitrogen in stratosphere, J. Geophys. Res., 77, 6589–6691, 1972.

Warneck, P. and Wurzinger, C.: Product quantum yields for the 305-nm photodecomposition of NO3- in aqueous-solution, J. Phys. Chem., 92, 6278–6283, https://doi.org/10.1021/j100333a022, 1988.

Wegner, T.: Chlorine activation and heterogeneous chemistry in the polar stratosphere: model simulations, in-situ- and satellite observations, Ph.D. thesis, Bergische Universität Wuppertal, URN: 468-20130607-103013-5, 2013.

Wegner, T., Grooß, J.-U., von Hobe, M., Stroh, F., Sumińska-Ebersoldt, O., Volk, C. M., Hösen, E., Mitev, V., Shur, G., and Müller, R.: Heterogeneous chlorine activation on stratospheric aerosols and clouds in the Arctic polar vortex, Atmos. Chem. Phys., 12, 11 095–11 106, https://doi.org/10.5194/acp-12-11095-2012, 2012.

Wegner, T., Kinnison, D. E., Garcia, R. R., and Solomon, S.: Simulation of polar stratospheric clouds in the specified dynamics version of the whole atmosphere community climate model, J. Geophys. Res., pp. 4991–5002, https://doi.org/10.1002/jgrd.50415, 2013.

Wild, O. and Prather, M. J.: Excitation of the primary tropospheric chemical mode in a global three-dimensional model, J. Geophys. Res., 105, 24 647–24 660, https://doi.org/10.1029/2000JD900399, 2000.

Wingen, L. M., Moskun, A. C., Johnson, S. N., Thomas, J. L., Roeselová, M., Tobias, D. J., Kleinman, M. T., and Finlayson-Pitts, B. J.: Enhanced surface photochemistry in chloride-nitrate ion mixtures, Phys. Chem. Chem. Phys., 10, 5668–5677, https://doi.org/10.1039/b806613b, 2008.

WMO: Scientific assessment of ozone depletion: 2014, Global Ozone Research and Monitoring Project–Report No. 55, Geneva, Switzerland, 2014.

Wohltmann, I., Lehmann, R., and Rex, M.: A quantitative analysis of the reactions involved in stratospheric ozone depletion in the polar vortex core, Atmos. Chem. Phys., 17, 10 535–10 563, https://doi.org/10.5194/acp-17-10535-2017, https://www.atmos-chem-phys.net/17/10535/2017/, 2017.

Wohltmann, I., Lehmann, R., and Rex, M.: The Lagrangian chemistry and transport model ATLAS: simulation and validation of stratospheric chemistry and ozone loss in the winter 1999/2000, Geosci. Model Dev., 3, 585–601, https://doi.org/10.5194/gmd-3-585-2010, 2010.

Ye, C., Zhou, X., Pu, D., Stutz, J., Festa, J., Spolaor, M., Tsai, C., Cantrell, C., Mauldin, III, R. L., Campos, T., Weinheimer, A., Hornbrook, R. S., Apel, E. C., Guenther, A., Kaser, L., Yuan, B., Karl, T., Haggerty, J., Hall, S., Ullmann, K., Smith, J. N., Ortega, J., and Knote, C.: Rapid cycling of reactive nitrogen in the marine boundary layer, Nature, 532, 489–491, https://doi.org/10.1038/nature17195, 2016.

Atmos. Chem. Phys. Discuss., https://doi.org/10.5194/acp-2018-202
Manuscript under review for journal Atmos. Chem. Phys.
Discussion started: 28 February 2018

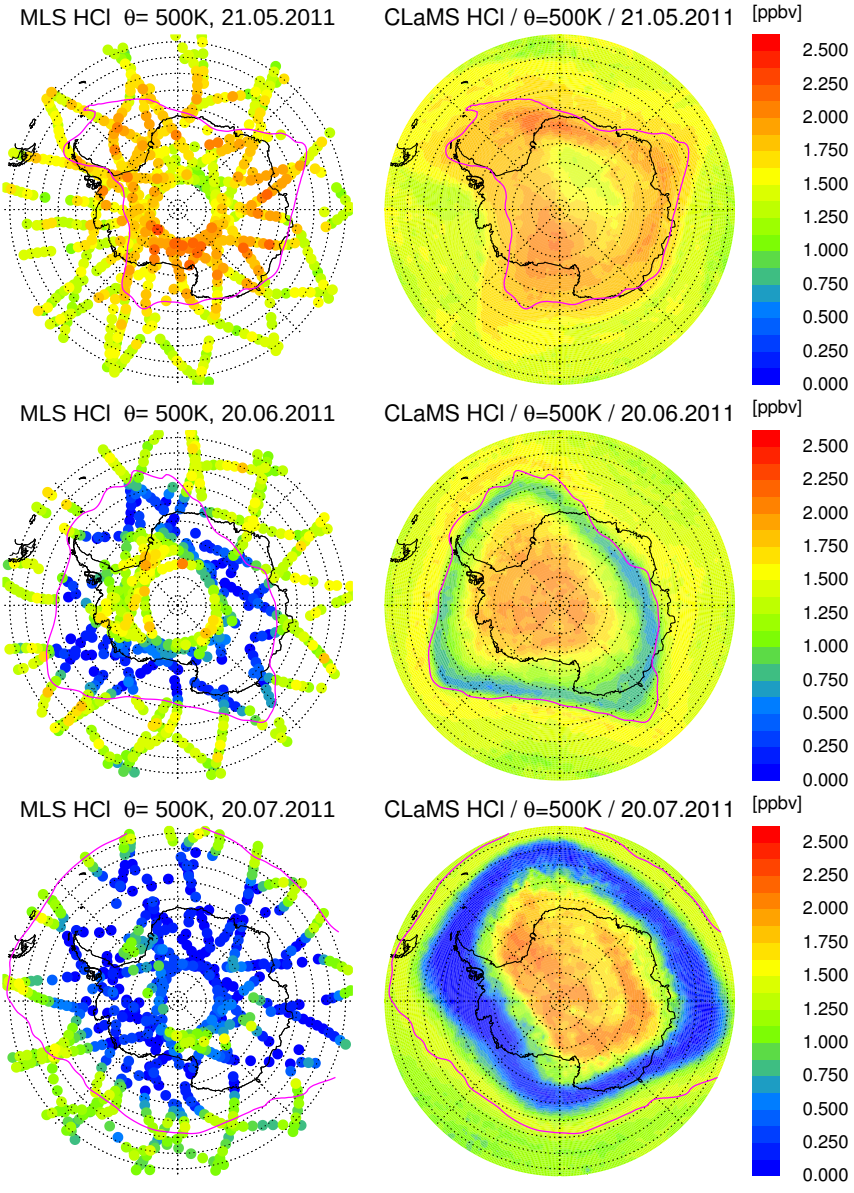

Figure 1. Time series of orthographic projection of MLS observations (left) and CLaMS simulations (right) of HCl mixing ratios on the 500 K potential temperature level. These maps are shown for the 21 May (top), 20 June (middle), and 20 July 2011 (bottom), respectively. The pink line depicts the edge of the polar vortex according to Nash et al. (1996).

Atmos. Chem. Phys. Discuss., https://doi.org/10.5194/acp-2018-202
Manuscript under review for journal Atmos. Chem. Phys.
Discussion started: 28 February 2018

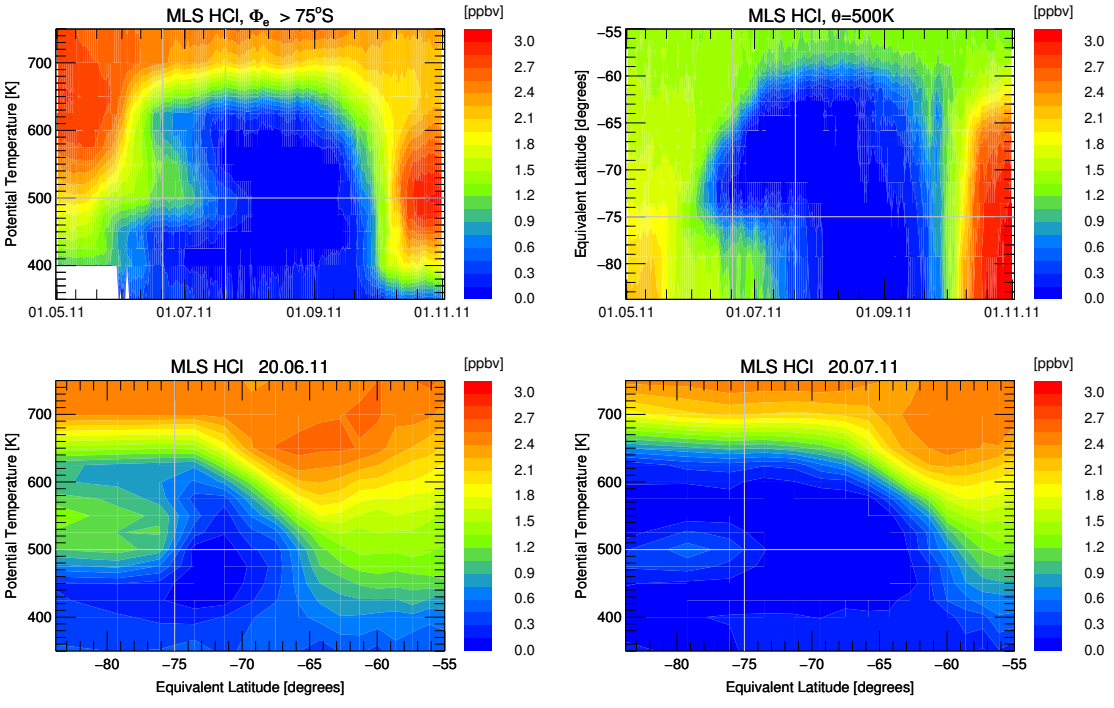

Figure 2. Depiction of MLS HCl mixing ratio data averaged in equivalent latitude/potential temperature space. The top left panel shows the vortex core average for equivalent latitudes pole-ward of 75°S as a function of time and potential temperature. The top right panel shows the development on the 500 K potential temperature level. The bottom two panels show a snapshot of this average on 20 June and 20 July 2011. Grey lines on the panels indicate the cuts or borders displayed in the other panels of this figure.

Atmos. Chem. Phys. Discuss., https://doi.org/10.5194/acp-2018-202
Manuscript under review for journal Atmos. Chem. Phys.
Discussion started: 28 February 2018

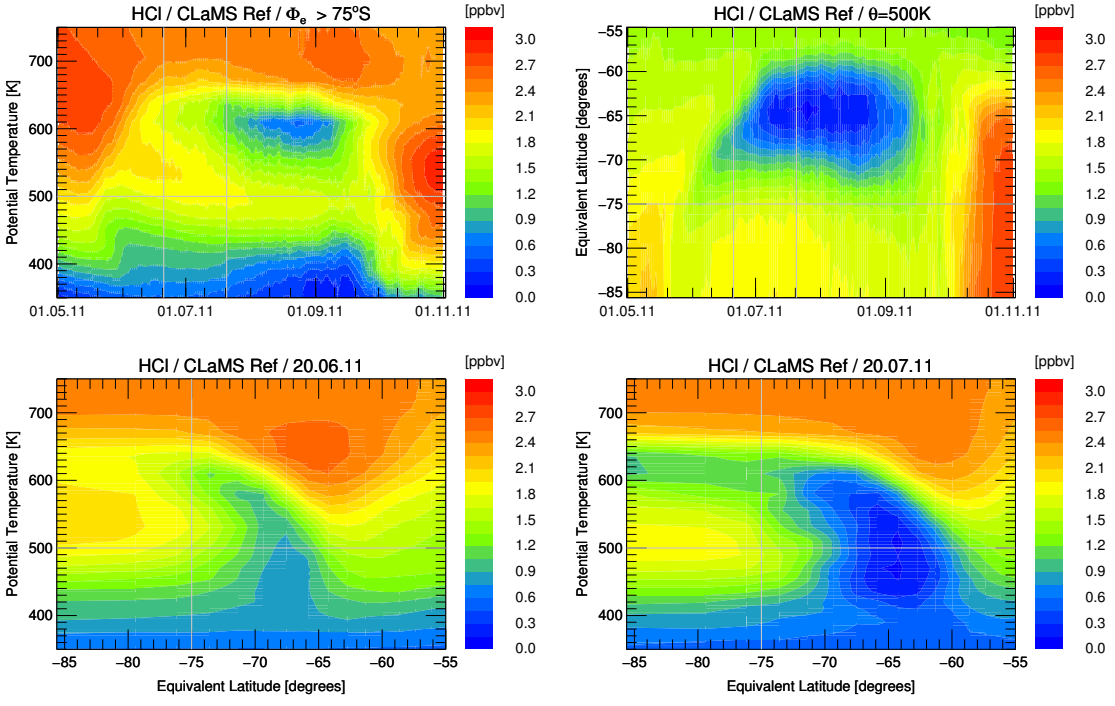

Figure 3. CLaMS simulation results for HCl averaged in equivalent latitude/potential temperature space displayed as in Fig. 2.

Atmos. Chem. Phys. Discuss., https://doi.org/10.5194/acp-2018-202
Manuscript under review for journal Atmos. Chem. Phys.
Discussion started: 28 February 2018

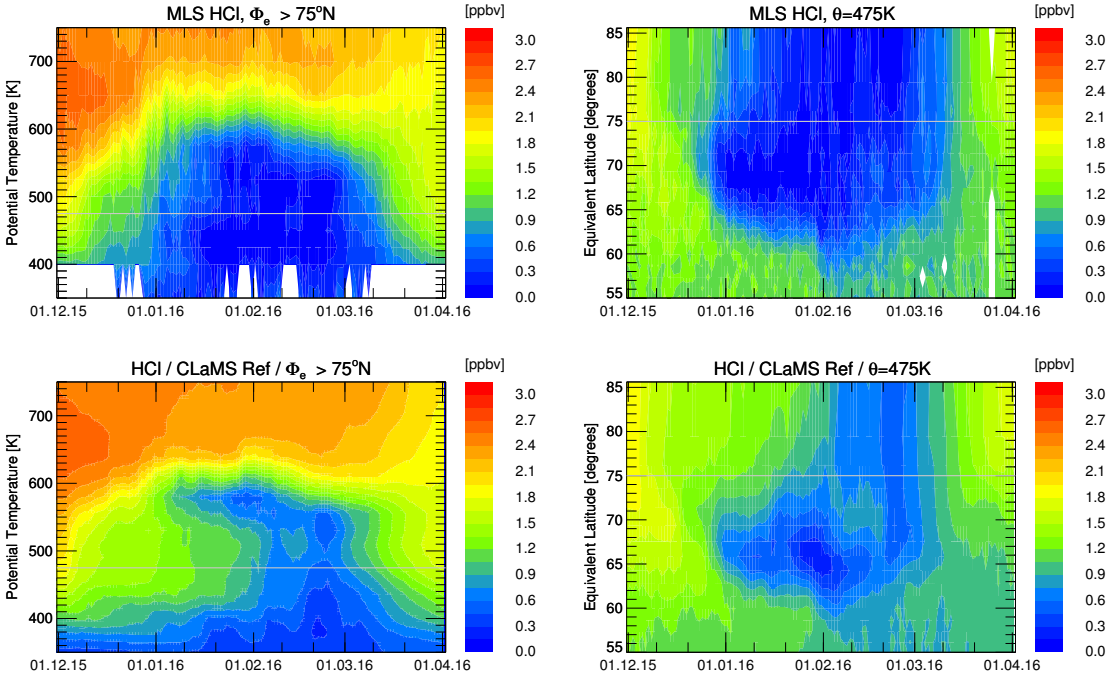

Figure 4. Similar results than displayed in Figs. 2 and 3 for the simulation of the Arctic winter 2016. The top two panels depict the MLS HCl mixing ratio data averaged in equivalent latitude/potential temperature space for the vortex core ($\Phi_e > 75^\circ$N, top left) and the development on the 475 K potential temperature level. The bottom two panels show the corresponding model results from CLaMS. Grey lines on the panels indicate the cuts or borders displayed in the other panels of this figure.

Atmos. Chem. Phys. Discuss., https://doi.org/10.5194/acp-2018-202
Manuscript under review for journal Atmos. Chem. Phys.
Discussion started: 28 February 2018

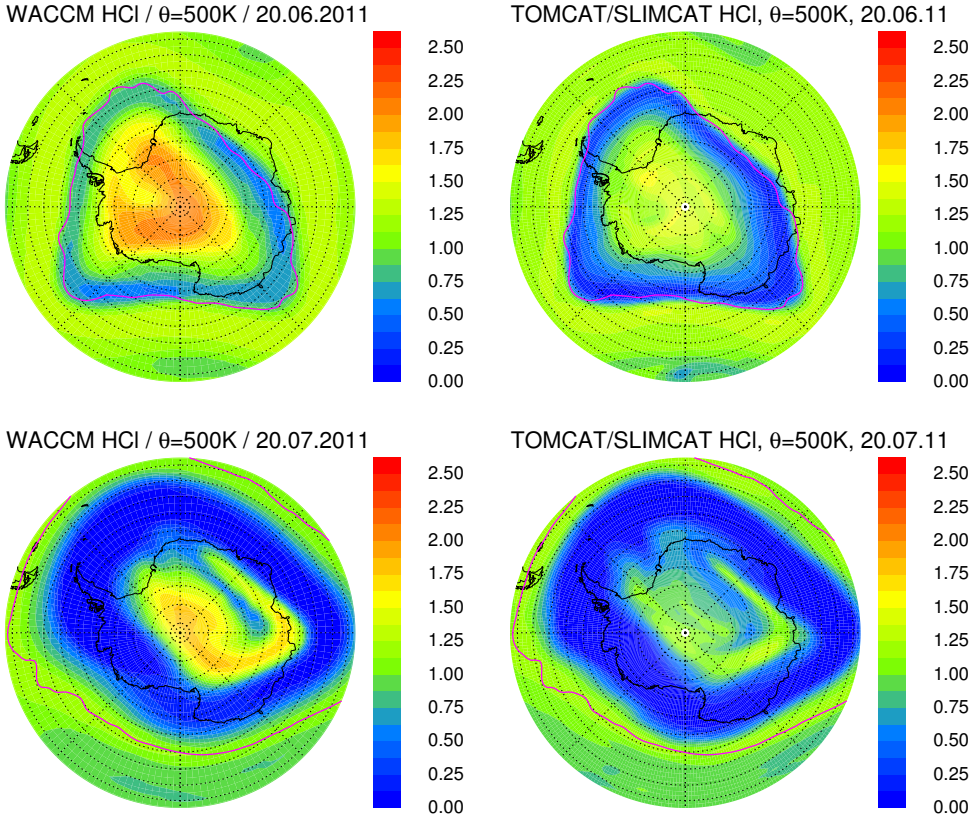

Figure 5. WACCM (left panels) and TOMCAT/SLIMCAT (right panels) simulation results for HCl on the 500 K potential temperature surface for 20 June (top panels) and 20 July 2011 (bottom panels) displayed as in Fig. 1.

Atmos. Chem. Phys. Discuss., https://doi.org/10.5194/acp-2018-202
Manuscript under review for journal Atmos. Chem. Phys.
Discussion started: 28 February 2018

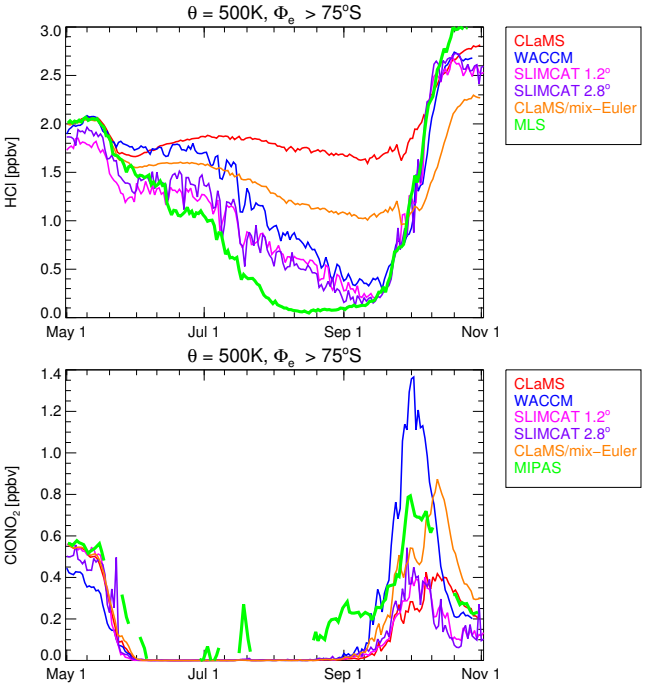

Figure 6. Vortex core averages ($\Phi_e > 75°$S) on the 500 K isentrope for HCl (top) and $ClONO_2$ (bottom) for different model simulations. Observations of MLS and MIPAS are shown as green lines. The red line corresponds to CLaMS, the blue line corresponds to WACCM, pink and purple lines correspond to TOMCAT/SLIMCAT simulations with horizontal resolution 1.2° and 2.8°, respectively. The orange line corresponds to the CLaMS simulation mix-Euler, in which additional artificial mixing was applied.

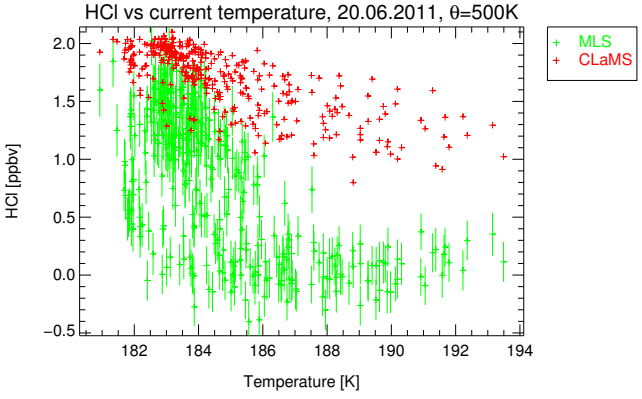

Figure 7. MLS observations of HCl mixing ratio on 20 June 2011 in the vortex core ($\Phi_e > 75°$S) on the 500 K potential temperature level. The individual data points are plotted as function of temperature given by ERA-Interim (green symbols). The error bars show the given measurement precision. The corresponding CLaMS results are given as red symbols.

Atmos. Chem. Phys. Discuss., https://doi.org/10.5194/acp-2018-202
Manuscript under review for journal Atmos. Chem. Phys.
Discussion started: 28 February 2018

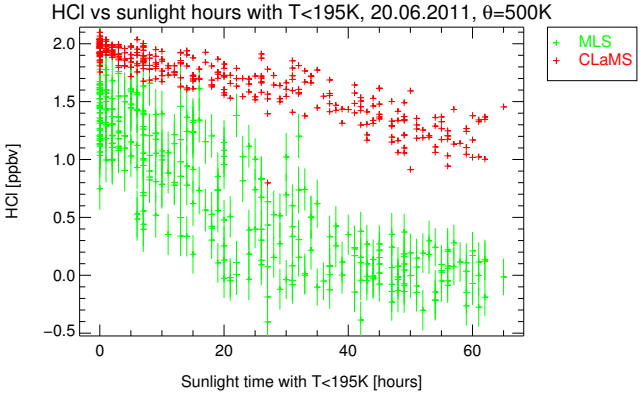

Figure 8. MLS observations of HCl mixing ratio that are also displayed in Fig.8 plotted against sunlight time with temperatures below 195 K derived from the backward trajectories (green symbols) and the corresponding CLaMS results (red symbols).

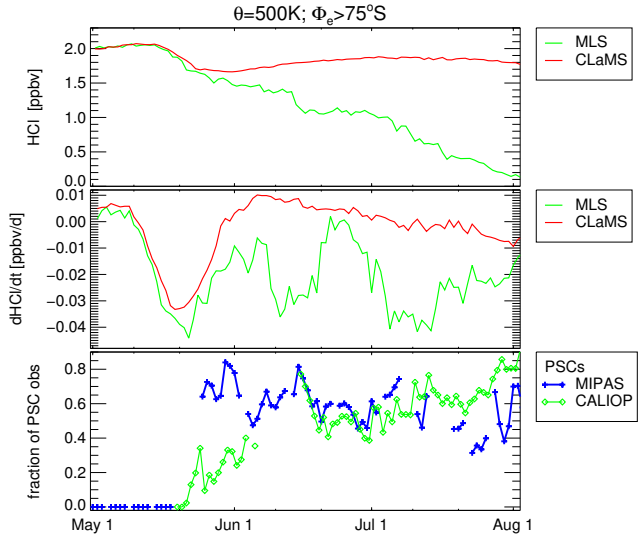

Figure 9. Vortex core averages (Φ_e >75°S, θ=500 K) of HCl, its time derivative and PSC occurrence frequency. The top panel shows HCl mixing ratios from CLaMS and MLS. The middle panel shows the corresponding time derivative dHCl/dt (smoothed as a 6-day running mean). The bottom panel shows the fraction of MIPAS and CALIOP observations with Φ_e >75°S on the 500 K potential temperature level that are classified as PSCs. The symbols are connected with coloured lines except for days without PSC information.

Atmos. Chem. Phys. Discuss., https://doi.org/10.5194/acp-2018-202
Manuscript under review for journal Atmos. Chem. Phys.
Discussion started: 28 February 2018

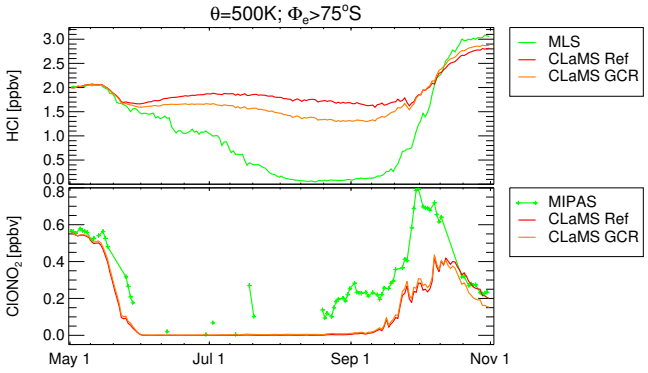

Figure 10. Average mixing ratios in the vortex core (Φ_e >75°S, θ=500 K) of HCl (top panel) and $ClONO_2$ (bottom panel). Green lines show MLS and MIPAS observations, respectively. CLaMS results are shown for the reference simulations (red) and the simulation with incorporated ionisation from galactic cosmic rays (GCR, orange).

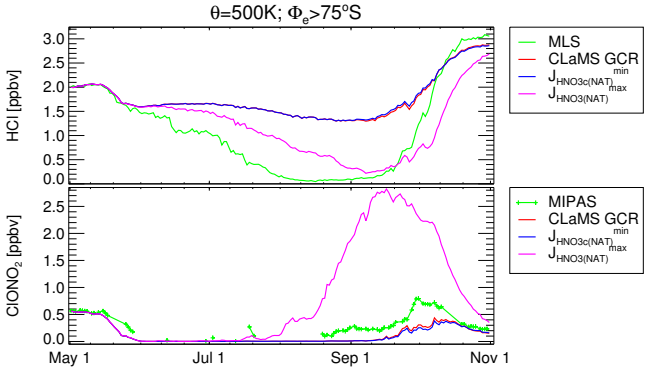

Figure 11. Average mixing ratios in the vortex core (Φ_e >75°S, θ=500 K) of HCl (top panel) and $ClONO_2$ (bottom panel). Green lines show MLS and MIPAS observations, respectively. The red line shows the CLaMS simulation including GCR induced ionisation. The blue and pink lines correspond to simulations with additional photolysis of particulate HNO_3 using the lower and upper estimate, respectively as described in the text.

Atmos. Chem. Phys. Discuss., https://doi.org/10.5194/acp-2018-202
Manuscript under review for journal Atmos. Chem. Phys.
Discussion started: 28 February 2018

Atmospheric Chemistry and Physics Discussions

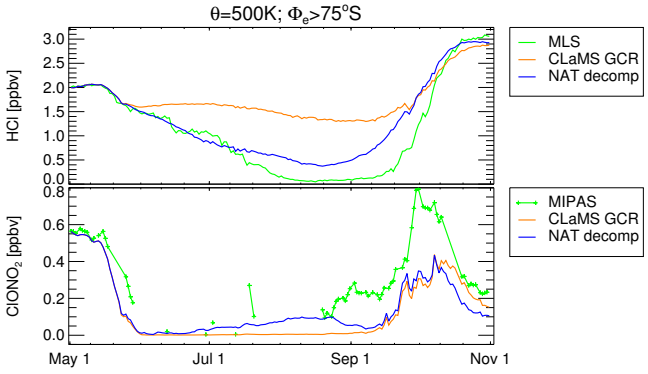

Figure 12. As Fig. 10 but for CLaMS simulation with hypothetical NAT decomposition. CLaMS results are shown for the GCR simulation (orange) and the simulation NAT decomp (blue).

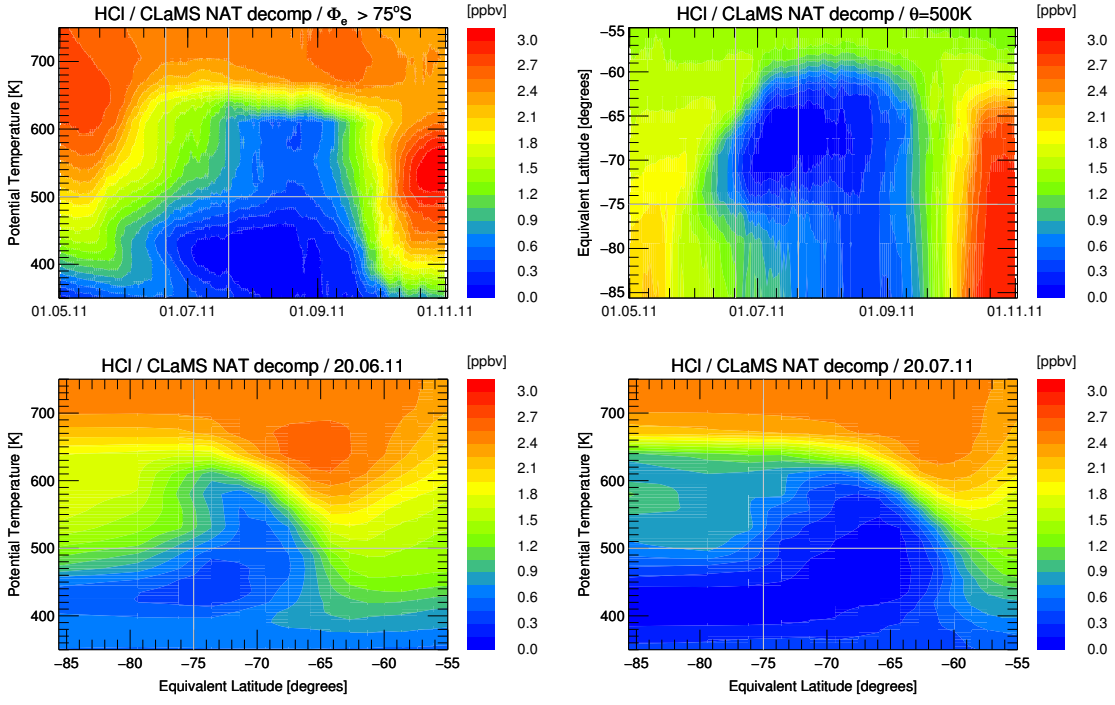

Figure 13. CLaMS simulation results for HCl of the sensitivity simulation NAT decomp averaged in equivalent latitude/potential temperature space displayed as in Figs. 2 and 3.

Atmos. Chem. Phys. Discuss., https://doi.org/10.5194/acp-2018-202
Manuscript under review for journal Atmos. Chem. Phys.
Discussion started: 28 February 2018

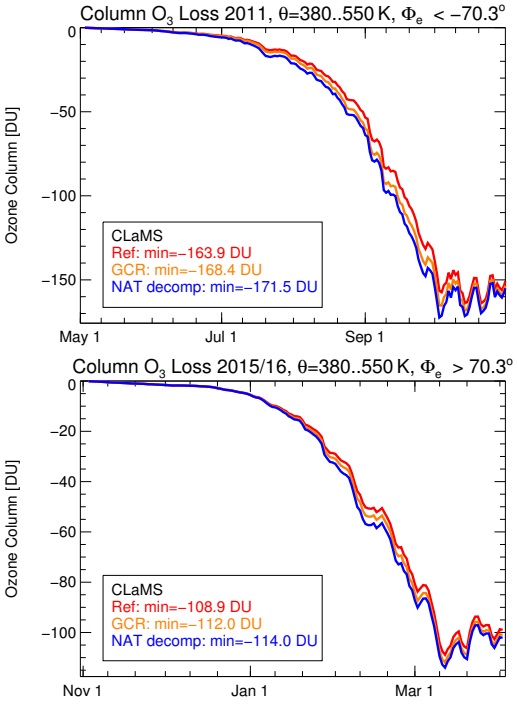

Figure 14. Simulated column ozone loss between 380 K and 550 K potential temperature for the Antarctic winter 2011 (top panel) and the Arctic winter 2015/2016 (bottom panel). The results are shown for different sensitivity simulations. Red lines correspond to the reference simulation, orange lines to the simulation including GCR-induced ionisation, and blue lines to the simulation NAT decomp. The legend also indicates the maximum column ozone loss amount of each simulation.